Inorg. Chem. **2007**, *46*, 6056–6068

Copper(I) Complex O_2-Reactivity with a N_3S Thioether Ligand: a Copper–Dioxygen Adduct Including Sulfur Ligation, Ligand Oxygenation, and Comparisons with All Nitrogen Ligand Analogues

Dong-Heon Lee,[†,‡] Lanying Q. Hatcher,[†] Michael A. Vance,[§] Ritimukta Sarangi,[§] Ashley E. Milligan,[§] Amy A. Narducci Sarjeant,[†] Christopher D. Incarvito,[£] Arnold L. Rheingold,[£,||] Keith O. Hodgson,[§] Britt Hedman,[§] Edward I. Solomon,[§] and Kenneth D. Karlin*[,†]

Department of Chemistry, The Johns Hopkins University, Baltimore, Maryland 21218, Department of Chemistry, Chonbuk National University, Jeonju, Korea, 561-756, Department of Chemistry, Stanford University, Stanford, California 94305, Department of Chemistry, University of Delaware, Newark, Delaware 19716

Received March 21, 2007

In order to contribute to an understanding of the effects of thioether sulfur ligation in copper–O_2 reactivity, the tetradentate ligands L^{N3S} (2-ethylthio-*N*,*N*-bis(pyridin-2-yl)methylethanamine) and $L^{N3S'}$(2-ethylthio-*N*,*N*-bis(pyridin-2-yl)ethylethanamine) have been synthesized. Corresponding copper(I) complexes, $[Cu^I(L^{N3S})]ClO_4$ (**1-ClO$_4$**), $[Cu^I(L^{N3S})]B(C_6F_5)_4$ (**1-B(C$_6$F$_5$)$_4$**), and $[Cu^I(L^{N3S'})]ClO_4$ (**2**), were generated, and their redox properties, CO binding, and O_2-reactivity were compared to the situation with analogous compounds having all nitrogen donor ligands, $[Cu^I(TMPA)(MeCN)]^+$ and $[Cu^I(PMAP)]^+$ (TMPA = tris(2-pyridylmethyl)amine; PMAP = bis[2-(2-pyridyl)ethyl]-(2-pyridyl)-methylamine). X-ray structures of **1-B(C$_6$F$_5$)$_4$**, a dimer, and copper(II) complex $[Cu^{II}(L^{N3S})(MeOH)](ClO_4)_2$ (**3**) were obtained; the latter possesses axial thioether coordination. At low temperature in CH_2Cl_2, acetone, or 2-methyltetrahydrofuran (MeTHF), **1** reacts with O_2 and generates an adduct formulated as an end-on peroxodicopper(II) complex $[\{Cu^{II}(L^{N3S})\}_2(\mu\text{-}1,2\text{-}O_2^{2-})]^{2+}$ (**4**)$\{\lambda_{max} = 530$ ($\epsilon \approx 9200$ M^{-1} cm^{-1}) and 605 nm ($\epsilon \approx 11\,800$ M^{-1} cm^{-1})$\}$; the number and relative intensity of LMCT UV–vis bands vary from those for $[\{Cu^{II}(TMPA)\}_2(O_2^{2-})]^{2+}$ $\{\lambda_{max} = 524$ nm ($\epsilon = 11\,300$ M^{-1} cm^{-1}) and 615 nm ($\epsilon = 5800$ M^{-1} cm^{-1})$\}$ and are ascribed to electronic structure variation due to coordination geometry changes with the L^{N3S} ligand. Resonance Raman spectroscopy confirms the end-on peroxo-formulation $\{\nu_{(O-O)} = 817$ cm^{-1} ($^{16-18}O_2$ $\Delta = 46$ cm^{-1}) and $\nu_{(Cu-O)} = 545$ cm^{-1} ($^{16-18}O_2$ $\Delta = 26$ cm^{-1})$\}$; these values are lower in energy than those for $[\{Cu^{II}(TMPA)\}_2(O_2^{2-})]^{2+}$ $\{\nu$(Cu–O) = 561 cm^{-1} and ν(O–O) = 827 cm^{-1}$\}$ and can be attributed to less electron density donation from the peroxide π^* orbitals to the Cu(II) ion. Complex **4** is the first copper–dioxygen adduct with thioether ligation; direct evidence comes from EXAFS spectroscopy {Cu K-edge; Cu–S = 2.4 Å}. Following a $[Cu^I(L^{N3S})]^+/O_2$ reaction and warming, the L^{N3S} thioether ligand is oxidized to the sulfoxide in a reaction modeling copper monooxygenase activity. By contrast, **2** is unreactive toward dioxygen probably due to its significantly increased Cu^{II}/Cu^I redox potential, an effect of ligand chelate ring size (in comparison to **1**). Discussion of the relevance of the chemistry to copper enzyme O_2-activation, and situations of biological stress involving methionine oxidation, is provided.

Introduction

The reactivity of copper(I) ion and molecular oxygen is of considerable interest for insights into intermediates involved in copper−protein O_2 binding/activation and for ultimately designing better/more specific or "green" practical reagents or catalysts for substrate oxidations. A great deal of knowledge has been obtained from (low-temperature) dioxygen reactivity studies of copper(I) complexes, and a number of spectroscopic/structural Cu_n-O_2(H) and reactivity types are now well established.[1−4] The first crystallographi-

* To whom correspondence should be addressed. E-mail: karlin@jhu.edu.
† The Johns Hopkins University.
‡ Chonbuk National University.
§ Stanford University.
£ University of Delaware.
|| Current address: Department of Chemistry and Biochemistry, University of California, San Diego, La Jolla, CA 92093-0332.

(1) Itoh, S. *Curr. Opin. Chem. Biol.* **2006**, *10*, 115−122.

10.1021/ic700541k CCC: $37.00
Published on Web 06/20/2007

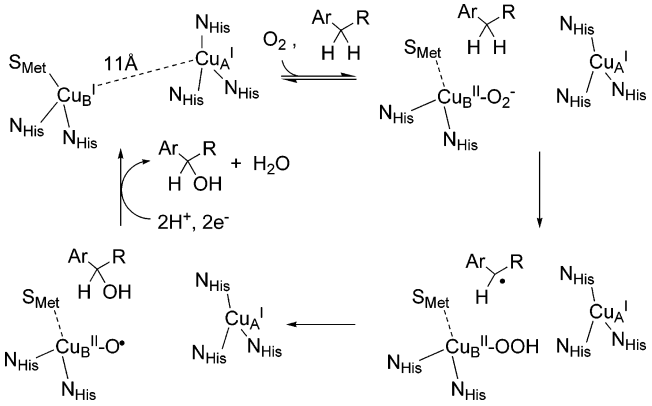

Figure 1. PHM active site and proposed mechanism of monooxygenase activity.

cally characterized dicopper−peroxide adduct came from early studies in our laboratory with the tetradentate amine ligand TMPA (tris(2-pyridyl)methylamine) (see below).[5,6] To date, most ligands utilized for Cu^I/O_2 reactivity studies are various forms of bi-, tri-, and tetradentate amine ligands, including alkyl, pyridyl, secondary, and tertiary amine donors, with each ligand feature in some way modulating the O_2 reactivity and subsequent Cu−dioxygen structure.[1−4]

However, other heteroatom ligand donors besides nitrogen can also coordinate to copper with the result being effective copper complex dioxygen activation/O-atom insertion reactions. Key biological examples occur at the active sites of dopamine β-hydroxylase (DβH) and peptidyl glycine α-hydroxylating monooxygenase (PHM), two enzymes involved in neurotransmitter biosynthesis/hormone regulation.[7] The two enzymes possess a high degree of sequence homology, each containing two functionally related but physically separated mononuclear copper centers. (X-ray structural information is available for PHM.[8−10]) Cu_M (also referred to as Cu_B), ligated by two histidines and a methionine residue, is the O_2 binding site forming a substrate H-atom abstracting active species. The other copper active site, Cu_H (also referred to as Cu_A), lies ∼11 Å away; it is ligated by three histidine residues and is the source of the second reducing electron required for the monooxygenase activity (Figure 1).

Theoretical/computational analyses profiling Cu^{II}−OOR (i.e., peroxide) reactivity[11−13] and separate mechanistic enzymological studies[7,14] have led to suggestions that a copper dioxygen adduct (a $Cu^{II}-O_2^-$ superoxide species) is the likely active site species effecting substrate hydrogen-atom abstraction, as in the mechanism outlined in Figure 1.[7,11,13,15] In fact, a recent protein X-ray structure[9] revealed a superoxide−copper moiety at the Cu_M site when in the presence of a bound substrate analogue (an inhibitor); this entity perhaps closely resembles the enzyme's catalytically active species. However, there are other computational investigations suggesting a 'cupryl' (Cu^{III}═O, $Cu^{II}-O^{\bullet}$, or $[CuO]^{2+}$)[16] H-atom abstracting agent (following O−O cleavage).[17,18]

The uncommon presence of a methionine ligand clearly plays a key role in tuning the dioxygen chemistry and effecting C−H hydroxylation. Yet the precise role and influence of thioether coordination on copper−dioxygen binding and chemistry[12,13,15] remains a subject of continuing interest. Why is the presence of a methionine (Met) so important to the coordination and/or electronic structure in this situation of oxidative reactivity, especially as copper ion can readily mediate the irreversible oxidation of organic sulfides to sulfoxides (or sulfones)?[19−21] Copper−dioxygen reactivity studies in cases with concurrent copper−sulfur coordination are uncommon in comparison to the extensive literature on Cu_nO_2 adducts with all nitrogen donors.[1−4] Certainly, spectroscopic, coordination, or redox studies on copper complexes with thioether ligands have been carried out. Rorabacher, Ochrymowycz, and co-workers[22−24] have carried out extensive coordination chemistry and redox studies with copper(I/II) thioether containing macrocycles. Other selected ligand examples are shown in Figure 2. Ligand **A** was utilized in conjunction with a bypyridine ligand to synthesize a copper(II) complex that structurally models the oxidized form of the Cu_M active sites of DβH and PHM with its axial Cu−thioether coordination.[25] The Met-derived thioether and amine containing ligand **B** (Figure 2) was

(2) Quant Hatcher, L.; Karlin, K. D. *J. Biol. Inorg. Chem.* **2004**, *9*, 669−683.
(3) Mirica, L. M.; Ottenwaelder, X.; Stack, T. D. P. *Chem. Rev.* **2004**, *104*, 1013−1045.
(4) Lewis, E. A.; Tolman, W. B. *Chem. Rev.* **2004**, *104*, 1047−1076.
(5) Tyeklár, Z.; Jacobson, R. R.; Wei, N.; Murthy, N. N.; Zubieta, J.; Karlin, K. D. *J. Am. Chem. Soc.* **1993**, *115*, 2677−2689.
(6) Jacobson, R. R.; Tyeklár, Z.; Karlin, K. D.; Liu, S.; Zubieta, J. *J. Am. Chem. Soc.* **1988**, *110*, 3690−3692.
(7) Klinman, J. P. *J. Biol. Chem.* **2006**, *281*, 3013−3016.
(8) Prigge, S. T.; Kolhekar, A.; Eipper, B. A.; Mains, R. E.; Amzel, M. *Science* **1997**, *278*, 1300−1305.
(9) Prigge, S. T.; Eipper, B.; Mains, R.; Amzel, L. M. *Science* **2004**, *304*, 864−867.
(10) Prigge, S. T.; Mains, R. E.; Eipper, B. A.; Amzel, L. M. *Cell. Mol. Life Sci.* **2000**, *57*, 1236−1259.
(11) Chen, P.; Fujisawa, K.; Solomon, E. I. *J. Am. Chem. Soc.* **2000**, *122*, 10177−10193.
(12) Chen, P.; Bell, J.; Eipper, B. A.; Solomon, E. I. *Biochemistry* **2004**, *43*, 5735−5747.
(13) Chen, P.; Solomon, E. I. *J. Am. Chem. Soc.* **2004**, *126*, 4991−5000.
(14) Evans, J. P.; Ahn, K.; Klinman, J. P. *J. Biol. Chem.* **2003**, *278*, 49691−49698.
(15) Chen, P.; Solomon, E. I. *Proc. Nat. Acad. Sci., U.S.A.* **2004**, *101*, 13105−13110.
(16) Decker, A.; Solomon, E. I. *Curr. Opin. Chem. Biol.* **2005**, *9*, 152−163.
(17) Yoshizawa, K.; Kihara, N.; Kamachi, T.; Shiota, Y. *Inorg. Chem.* **2006**, *45*, 3034−3041.
(18) Crespo, A.; Marti, M. A.; Roitberg, A. E.; Amzel, L. M.; Estrin, D. A. *J. Am. Chem. Soc.* **2006**, *128*, 12817−12828.
(19) Karlin, K. D.; Ghosh, P.; Cruse, R. W.; Farooq, A.; Gultneh, Y.; Jacobson, R. R.; Blackburn, N. J.; Strange, R. W.; Zubieta, J. *J. Am. Chem. Soc.* **1988**, *110*, 6769−6780.
(20) Taki, M.; Teramae, S.; Nagatomo, S.; Tachi, Y.; Kitagawa, T.; Itoh, S.; Fukuzumi, S. *J. Am. Chem. Soc.* **2002**, *124*, 6367−6377.
(21) Fujii, T.; Naito, A.; Yamaguchi, S.; Wada, A.; Funahashi, Y.; Jitsukawa, K.; Nagatomo, S.; Kitagawa, T.; Masuda, H. *Chem. Comm.* **2003**, 2700−2701.
(22) Ambundo, E. A.; Deydier, M.-V.; Grall, A. J.; Aguera-Vega, N.; Dressel, L. T.; Cooper, T. H.; Heeg, M. J.; Ochrymowycz, L. A.; Rorabacher, D. B. *Inorg. Chem.* **1999**, *38*, 4233−4242.
(23) Galijasevic, S.; Krylova, K.; Koenigbauer, M. J.; Jaeger, G. S.; Bushendorf, J. D.; Heeg, M. J.; Ochrymowycz, L. A.; Taschner, M. J.; Rorabacher, D. B. *Dalton Trans.* **2003**, 1577−1586.
(24) Rorabacher, D. B. *Chem. Rev.* **2004**, *104*, 651−697.
(25) Santra, B. K.; Reddy, P. A. N.; Nethaji, M.; Chakravarty, A. R. *Inorg. Chem.* **2002**, *41*, 1328−1332.

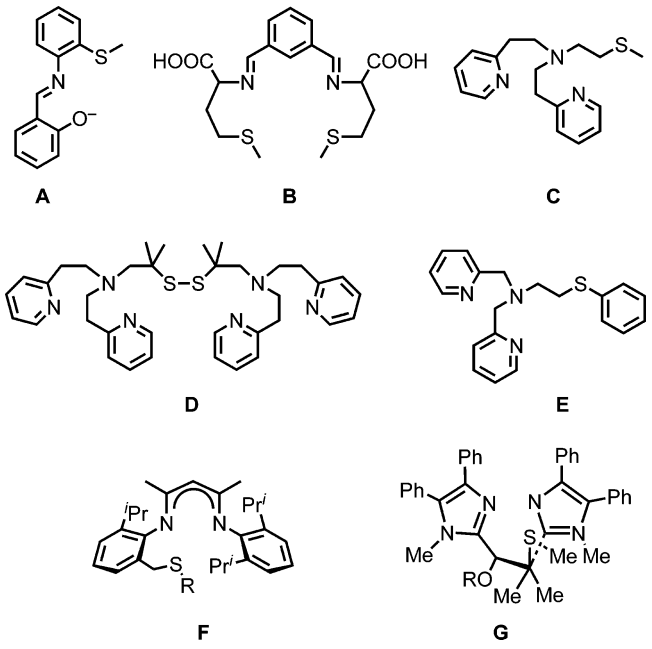

Figure 2. Selected thioether/disulfide ligands previously used for copper ligation and reactivity. See text.

synthesized by Casella and co-workers,[26,27] and they demonstrated that Cu^{I}_2/O_2 reactivity studies still allowed monooxygenase type chemistry, i.e., *m*-xylyl ligand hydroxylation; a minor fraction of the ligand was oxidized to the sulfoxide, attributable to the occurrence of a secondary process resulting from reaction of H_2O_2 and Cu^{II}. Reglier and co-workers[28] also observed ligand sulfoxidation from the reaction of a Cu^{II} complex with ligand **C** (Figure 2) with H_2O_2. However, no dioxygen intermediates were observed for the reaction of the Cu^{I} complex of the same ligand even at low temperature. Copper−hydroperoxo species generated from the reaction of H_2O_2 and copper(II) complexes (with ligands having a thioether sulfur coordination (ligands **D** and **E**, Figure 2) have been characterized in a few instances.[29,30] Recently, Tolman and co-workers[31] reported Cu^{I}/O_2 chemistry with ligand **F**; however, they observed that the thioether-S donor does not coordinate to copper in O_2-adduct products which form. Also, the group of Nicholas[32] employed a new imidazolyl N_2S-type ligand **G**; unfortunately, there was no copper(I)−dioxygen reactivity.

In an effort to extend copper−dioxygen reactivity to copper(I) complexes of thioether-amine ligands, we hereby describe the $Cu^{II/I}$ redox properties and dioxygen reactivity of the complexes $[Cu^{I}(L^{N3S})]ClO_4$ (**1-ClO$_4$**), $[Cu^{I}(L^{N3S})]B(C_6F_5)_4$ (**1-B(C$_6$F$_5$)$_4$**), and $[Cu^{I}(L^{N3S'})]ClO_4$ (**2**) (L^{N3S} = 2-ethylthio-*N*,*N*-bis(pyridin-2-yl)methylethanamine and $L^{N3S'}$ = 2-ethylthio-*N*,*N*-bis(pyridin-2-yl)ethylethanamine, Figure 3). By directly comparing them to analogous and well-studied systems, $[Cu^{I}(TMPA)(MeCN)]^+$ and $[Cu^{I}(PMAP)(MeCN)]^+$ (see Figure 3),[5,33,34] we seek to gain a better understanding of the role a thioether donor plays in the Cu^{I} redox properties and O_2-chemistry. The only difference between L^{N3S} and $L^{N3S'}$ is the alkyl spacer between the central amine and the pyridyl arms, which increases the copper chelate-rings size from five to six. We show that the thioether donor in L^{N3S} raises the redox potential of the Cu^{I} complex relative to analogues with only nitrogen donors, yet is still reactive toward O_2 at low temperature and forms an "end-on" μ-1,2-peroxodicopper(II) species with a new UV−vis absorption pattern. Furthermore, the room-temperature oxygenation of $[Cu^{I}(L^{N3S})]^+$ (**1**) behaves as a monooxygenase model system as the ligand becomes oxygenated in ca. 50% yield. By contrast, as expected from the observations of Reglier,[28] the "long armed" complex, **2**, is unreactive toward O_2. A preliminary report on some aspects of the work has appeared.[35]

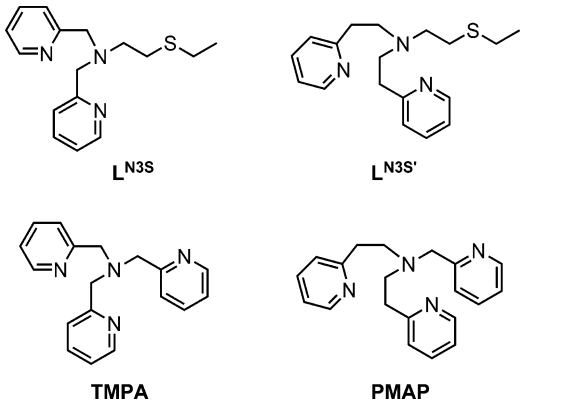

Figure 3. Tetradentate ligands for copper ion and chemistry discussed herein.

Experimental Section

General Considerations and Instrumentation. Resonance Raman (rR) data were collected using a Princeton Instruments ST-135 back-illuminated CCD detector on a Spex 1877 CP triple monochromator with 1200, 1800, and 2400 grooves/mm holographic spectrograph gratings. Excitation was provided by Coherent I90C-K Kr^+ and Innova Sabre 25/7 Ar^+ CW ion lasers. The spectral resolution was <2 cm^{-1}. Sample concentrations were $\sim$1 mM in Cu_2O_2. Samples were run at 77 K in a liquid N_2 finger Dewar (Wilmad) and were hand spun to minimize sample decomposition during scan collection. Isotopic substitution was achieved by oxygenating with $^{18}O_2$ (Icon, Summit, NJ). Elemental analyses were performed by Desert Analytics, Tucson, AZ. Mass Spectrometry was conducted at the mass spectrometry (MS) facility at either The

(26) Casella, L.; Gullotti, M.; Bartosek, M.; Pallanza, G.; Laurenti, E. *J. Chem. Soc. Chem. Commun.* **1991**, 1235−1237.
(27) Alzuet, G.; Casella, L.; Villa, M. L.; Carugo, O.; Gullotti, M. *J. Chem. Soc. Dalton Trans.* **1997**, 4789−4794.
(28) Champloy, F.; Benali-Cherif, N.; Bruno, P.; Blain, I.; Pierrot, M.; Reglier, M.; Michalowicz, A. *Inorg. Chem.* **1998**, *37*, 3910−3918.
(29) Ohta, T.; Tachiyama, T.; Yoshizawa, K.; Yamabe, T.; Uchida, T.; Kitagawa, T. *Inorg. Chem.* **2000**, *39*, 4358−4369.
(30) Kodera, M.; Kita, T.; Miura, I.; Nakayama, N.; Kawata, T.; Kano, K.; Hirota, S. *J. Am. Chem. Soc.* **2001**, *123*, 7715−7716.
(31) Aboelella, N. W.; Gherman, B. F.; Hill, L. M. R.; York, J. T.; Holm, N.; Young, V. G.; Cramer, C. J.; Tolman, W. B. *J. Am. Chem. Soc.* **2006**, *128*, 3445−3458.
(32) Zhou, L.; Powell, D.; Nicholas, K. M. *Inorg. Chem.* **2006**, *45*, 3840−3842.
(33) Schatz, M.; Becker, M.; Thaler, F.; Hampel, F.; Schindler, S.; Jacobson, R. R.; Tyeklár, Z.; Murthy, N. N.; Ghosh, P.; Chen, Q.; Zubieta, J.; Karlin, K. D. *Inorg. Chem.* **2001**, *40*, 2312−2322.
(34) Zhang, C. X.; Kaderli, S.; Costas, M.; Kim, E.-i.; Neuhold, Y.-M.; Karlin, K. D.; Zuberbühler, A. D. *Inorg. Chem.* **2003**, *42*, 1807−1824.
(35) Hatcher, L. Q.; Lee, D. H.; Vance, M. A.; Milligan, A. E.; Sarangi, R.; Hodgson, K. O.; Hedman, B.; Solomon, E. I.; Karlin, K. D. *Inorg. Chem.* **2006**, *45*, 10055−10057.

Johns Hopkins University or at The Ohio State University. CI spectra were acquired at the Johns Hopkins University MS facility using a VG70S double focusing magnetic sector mass spectrometer (VG Analytical, Manchester, UK, now Micromass/Waters) equipped with a Xe gas FAB gun (7.5 kV at 1 mA) and an off-axis electron multiplier. Samples were introduced into the CI source (block temperature = 200 °C) using a heated direct insertion probe using a deep quartz cup, at a rate of 0.5 °C/s. Methane reagent gas was used with an electron energy of 70 eV. High-boiling perfluorokerosene was used as the reference mass for accurate mass analyses. For accurate mass analyses, the matrix contained 10% PEG mass calibrant. Data was acquired using a MSS Data system (MasCom, Bremen, Germany) for subsequent processing. High-resolution electrospray ionization (ESI) mass spectrometry analyses were performed at the Ohio State University (MS) facility with a 3-T Finnigan FTMS-2000 Fourier transform mass spectrometer. Samples were sprayed from a commercial Analytical electrospray ionization source and then focused into the FTMS cell using a home-built set of ion optics. X-ray diffraction was performed at the X-ray diffraction facility either at the Johns Hopkins University or the University of Delaware. The X-ray absorption spectrum of $\{[(L^{N3S})Cu^{II}\}_2(\mu\text{-}1,2\text{-}O_2^{2-})]^{2+}$ (**4**) was carried out as previously described.[35] ^{1}H NMR and ^{13}C NMR spectra were measured on a Varian 400 MHz spectrometer and chemical shifts are reported in ppm (δ) downfield from an internal TMS reference. Infrared spectra of carbonyl adducts (as a solution in CH_2Cl_2) were recorded on a Mattson Instruments 4030 Galaxy Series FT-IR spectrometer using a solution IR cell. Low-temperature UV−vis spectra were taken either with a Hewlett-Packard model 8453 diode-array spectrophotometer equipped with a custom-made quartz Dewar filled with cold (−78 °C) methanol (maintained and controlled by a Neslab ULT-95 low-temperature circulator), or using a −78 °C methanol bath (CC-100 immersion cooler and Agitainor, Neslab) and taking measurements with a Cary 50 Bio spectrophotometer equipped with a fiber optic coupler (Varian) and a fiber optic dip probe (Hellma: 661.302-QX-UV-2mm-for-low-temperature). Air-sensitive solutions were prepared in a nitrogen atmosphere in a glove box (MBraun) and carried out in Schlenk 2 mm cuvettes (Quark) or custom-made Schlenk tubes designed for the dip probe (Chemglass: JHU-0407-271MS). rR spectroscopy measurements were undertaken on a Princeton Instruments ST-135 back-illuminated CCD detector on a Spex 1877 CP triple monochromator with 1200, 1800, and 2400 grooves/mm holographic spectrograph gratings. Excitation was provided by a Coherent I90C-K Kr^+ ion laser (λ_{ex} = 620). The spectral resolution was <2 cm^{-1}. Sample concentrations were ∼3 mM in Cu_2O_2. Samples were run at 77 K in a liquid N_2 finger Dewar (Wilmad) and were hand spun to minimize sample decomposition during scan collection. Isotopic substitution was achieved by oxygenating with $^{18}O_2$ (Icon). X-Band EPR spectra were recorded on a Bruker EMX CW-EPR spectrometer. The cavity was maintained at ∼4 K with the use of a He cryostat. Cyclic voltammetry measurements were undertaken in freshly distilled acetonitrile with a BAS 100B electrochemical analyzer with a glassy carbon working electrode and a platinum wire auxiliary electrode. Potentials were recorded versus a $Ag/AgNO_3$ electrode. The voltammograms are plotted versus the $Fe(cp)_2^{+/0}$ potential which was measured as an external standard. Scans were run at 50−500 mV/s under an argon atmosphere using ca. 0.1 M $[Bu_4N][PF_6]$ as the supporting electrolyte.

XAS Data Acquisition. The X-ray absorption spectra of **4** and of the temperature-induced decay product of **4** were measured at the Stanford Synchrotron Radiation Laboratory on the focused 16-pole 2.0 T wiggler beam line 9-3 under standard ring conditions of 3 GeV and 80−100 mA. A Si(220) double crystal monochromator was used for energy selection. A Rh-coated harmonic rejection mirror and a cylindrical Rh-coated bent focusing mirror were used for beam line 9-3 to reject components of higher harmonics. A 2-MeTHF solution of **4** was loaded into a lucite XAS cell with a precooled syringe. The temperature of the solution was maintained below −120 °C during this process. The sample was immediately frozen thereafter and stored under liquid N_2. During data collection, it was maintained at a constant temperature of 10 K using an Oxford Instruments CF 1208 liquid helium cryostat. Fluorescence mode was used to measure data to k = 13.4 $Å^{-1}$ employing a Canberra Ge 30-element solid array detector. Internal energy calibration was accomplished by simultaneous measurement of the absorption of a Cu foil placed between two ionization chambers situated after the sample.[36] The first inflection point of the foil spectrum was assigned to 8980.3 eV. Data represented here are an eight-scan (**4**) and six-scan (temperature induced decay product of **4**) average spectrum, which was processed by fitting a second-order polynomial to the pre-edge region and subtracting this from the entire spectrum as background. A three-region spline of orders 2, 3, and 3 was used to model the smoothly decaying post-edge region. The data were normalized by subtracting the cubic spline and by assigning the edge jump to 1.0 at 9000 eV using the PySpline program.[37] Theoretical EXAFS signals $\chi(k)$ were calculated using *FEFF* (version 7.0)[38,39] and fit to the data using EXAFSPAK.[40] The structural parameters varied during the fitting process were the bond distance (R) and the bond variance σ^2, which is related to the Debye−Waller factor resulting from thermal motion, and static disorder. The nonstructural parameter E_0 (the energy at which k = 0) was also allowed to vary but was restricted to a common value for every component in a given fit. Coordination numbers were systematically varied in the course of the fit but were fixed within a given fit.

Synthesis of Ligands and Copper Complexes. Reagents and solvents used were of commercially available reagent quality unless otherwise stated. Methylene chloride, methanol, and diethyl ether were purified/dried by passing through a double alumina column solvent purification system by Innovative Technologies, Inc. Methanol was also distilled from Mg turnings. Acetone was distilled from Drierite under argon. $[Cu^I(CH_3CN)_4]ClO_4$ was synthesized according to previously published procedures.[41,42] Air-sensitive compounds were synthesized and handled under an argon atmosphere using standard Schlenk techniques and stored in an MBraun drybox filled with N_2. Deoxygenation of solvents was achieved either by bubbling argon through the solution for 30−45 min or by three freeze−pump−thaw cycles.

2-Ethylthio-*N*,*N*-bis(pyridin-2-yl)methylethanamine (L^{N3S}). These ligands have in fact been previously reported[22] and also described in our preliminary communication.[34]

2-Ethylthio-*N*,*N*-bis(pyridin-2-yl)ethylethanamine ($L^{N3S'}$). $L^{N3S'}$ was synthesized according to the method of Ambundo, et al.[22] *N*,*N*-

(36) DuBois, J. L.; Mukherjee, P.; Stack, T. D. P.; Hedman, B.; Solomon, E. I.; Hodgson, K. O. *J. Am. Chem. Soc.* **2000**, *122*, 5775−5787.
(37) Tenderholt, A. *PySpline*; Stanford University: Stanford, CA, 2005.
(38) Deleon, J. M.; Rehr, J. J.; Zabinsky, S. I.; Albers, R. C. *Phys. Rev. B* **1991**, *44*, 4146−4156.
(39) Rehr, J. J.; Deleon, J. M.; Zabinsky, S. I.; Albers, R. C. *J. Am. Chem. Soc.* **1991**, *113*, 5135−5140.
(40) George, G. N. *EXAFSPAK*; *EDG_FIT*; Stanford Synchrotron Radiation Laboratory: Stanford, CA, 2000.
(41) Liang, H.-C.; Kim, E.; Incarvito, C. D.; Rheingold, A. L.; Karlin, K. D. *Inorg. Chem.* **2002**, *41*, 2209−2212.
(42) Liang, H.-C.; Karlin, K. D.; Dyson, R.; Kaderli, S.; Jung, B.; Zuberbühler, A. D. *Inorg. Chem.* **2000**, *39*, 5884−5894.

bis-(2-pyridin-2-yl-ethyl)-amine[43] (9.21 g, 40.4 mmol) and 1-chloro-2-ethylthioethane (5.0 g, 40.1 mmol) were dissolved in toluene. Excess $NaHCO_3$ was added, and the reaction was heated to 80 °C for 3 days. The reaction was then filtered and the solvent removed in vacuo to isolate the crude oil. The product was purified by column chromatography using 2.5% to 4% (incrementally) MeOH/CH_2Cl_2 on silica gel. ^{1}H NMR ($CDCl_3$): δ 8.52 (2 H, py-6, d, J = 4.8 Hz), 7.55 (2 H, py-5, t, J = 7.8 Hz), 7.10 (2 H, py-3,4 m), 2.94 (8 H, m), 2.79 (2 H, m), 2.52 (4 H, m), 1.23 (3 H, t, J = 7.4 Hz). High-resolution ESI-MS m/z ($M + H^+$): Calcd: 316.184193, Found: 316.18469.

$[Cu^I(L^{N3S})]ClO_4$ (1-ClO_4) and $[Cu^I(L^{N3S})]B(C_6F_5)_4$ (1-$B(C_6F_5)_4$). The syntheses of these complexes were described in our preliminary communication.[35]

$[Cu^I(L^{N3S'})]ClO_4$ (2). Under an Ar atmosphere, $L^{N3S'}$ (0.366 g, 1.16 mmol) in 10 mL of MeCN was added with stirring to solid $[Cu(MeCN)_4]ClO_4$ (0.375 g, 1.16 mmol). The solution was stirred for 30 min and was then filtered through a medium-porosity frit to collect a clear, golden-yellow solution. It was layered with deoxygenated ether at 0 °C after which a brown oil separated from the solution. The organic solvents were decanted and the oil was redissolved in 2 mL of dichloromethane. To this solution was added 5 mL of petroleum ether, and oil separated from solution which was dried in vacuo to collect 0.250 g (45% yield) of yellow solid. Anal. Calcd for ($C_{18}H_{25}ClCuN_3O_4S$): C, 45.18; H, 5.27; N, 8.78. Found: C, 45.60; H, 5.15; N, 8.94. ^{1}H NMR (CD_3CN): δ 8.59 (2 H, d, J = 5.0 Hz), 7.81 (4 H, m), 2.93 (4 H, br m), 2.83 (4 H, br m), 2.77 (8 H, m), 2.08 (2 H, br s), 2.65 (2 H, m), 1.21 (3 H, t, J = 7.4 Hz).

$[Cu^{II}(L^{N3S})(MeOH)](ClO_4)_2$ (3). $Cu^{II}(ClO_4)_2 \cdot 6H_2O$ (0.310 g, 0.84 mmol) was added to 0.240 g of L^{N3S} in 5 mL of acetonitrile, and the mixture was stirred for 2 h. Then, 50 mL of diethyl ether was added in order to precipitate the copper(II) complex. After sitting overnight, a deep blue oil separated out from the solution. The oil was washed with ether and was then crystallized by dissolving it in 5 mL of methanol layered with ca. 10 mL of ether. A blue crystalline solid (0.3571 g, 73% yield) was collected. The crystals were of suitable quality for X-ray crystallography. Anal. Calcd for ($C_{17}H_{25}Cl_2CuN_3O_9S$): C, 35.09; H, 4.33; N, 7.22. Found: C, 34.78; H, 4.26; N, 7.29. UV−vis (MeOH) 670 nm (ϵ = 90 M^{-1} cm^{-1}): EPR (4K, DMF/toluene frozen glass): $g_\perp = 2.079$, $g_{||} = 2.257$, $A_{||} = 181 \times 10^{-4}$ cm^{-1}, also see Figure S1.

Carbon Monoxide Binding and In Situ Cu−CO IR Monitoring. Using a syringe, excess CO(g) was bubbled through a 5.0 mM solution of $[Cu^I(L^{N3S})]ClO_4$ (**1-ClO_4**) in degassed dichloromethane or acetonitrile. The immediate formation of the carbonyl complex $[Cu^I(L^{N3S})(CO)]^+$ (**1-CO**), was observed by the appearance of a corresponding CO stretching frequency: ν_{CO} = 2094 cm^{-1} in acetonitrile (see Supporting Information, Figure S1) and 2096 cm^{-1} (data not shown) in dichloromethane. The CO stretch was identified by comparing with the IR spectrum of the starting material, **1-ClO_4**, recorded under the same conditions.

Dioxygen reactivity of 1 and 2. In the glove box, the copper(I) complex solutions were prepared by dissolving in CH_2Cl_2, and reaction flasks sealed with a rubber septa. Out on the benchtop, O_2 was bubbled through the solution for ca. 60 s at room temperature. The solution quickly changed from yellow to aqua. After 5 min, the metal ion was then removed from the ligand by shaking the organic layer with 35% NH_4OH. The organic layer was then dried over $MgSO_4$ and filtered, and the solvent was removed by rotary evaporation. The remaining yellow oil was analyzed by ^{1}H NMR spectroscopy. The oxidized ligand, L^{N3Sox}, was purified by column chromatography on silica gel with 5% CH_3OH in CH_2Cl_2 and was identified as the sulfoxide derivative of L^{N3S} by ^{1}H NMR and high-resolution mass spectrometry. The ^{1}H NMR spectrum indicated a chiral center according to the splitting of the methyl protons adjacent to the thioether-S atom, suggesting that the lone pairs on the sulfur were no longer equivalent and had been modified. The mass spectrum displayed a mass of 16 units more than L^{N3S} and fit the calculated value for the ligand sulfoxide. Characterization for L^{N3Sox}: ^{1}H NMR ($CDCl_3$): δ 8.52 (2 H, py-6, d, J = 4.0 Hz), 7.67 (2 H, py-5, td, J = 7.6, 2.0 Hz), 7.50 (2 H, py-3 d, J = 4.3 Hz), 7.14 (2 H, py-4, m), 3.87 (4 H, s), 3.06 (2 H, m), 2.87 (2 H, m), 2.63 (2 H, m), 1.24 (3 H, t, J = 7.4 Hz). CI−MS m/z ($M + H^+$): Calcd: 304.14836, Found: 304.14788 (Using labeled $^{18}O_2$, found: 306.15329, 58% $^{18}O_2$ incorporation based on the 304 vs 306 m/z peak intensities). IR: Following an oxidation reaction, the yields of ligand sulfoxidation was found to be 44% based on the relative ^{1}H NMR signal intensities for L^{N3Sox} and L^{N3S}. The reaction was repeated in triplicate.

H_2O_2 Reactivity of 3. The copper(II) complex was dissolved in methanol. Then, 10 equiv of H_2O_2 was added. The reaction was stirred for 2 h at room temperature during which time the color remained blue. The methanol was then removed by rotary evaporation, and the blue residue was redissolved in CH_2Cl_2. The metal was then removed from the ligand by shaking the organic layer with 35% NH_4OH. The organic layer was then dried, and the solvent was removed by rotary evaporation. The remaining yellow oil was analyzed by ^{1}H NMR spectroscopy and identified as L^{N3Sox}. Following an oxidation reaction, the yields of ligand sulfoxidation was found to be 74% based on the relative ^{1}H NMR-signal intensities for L^{N3Sox} and L^{N3S}. The reaction was repeated in triplicate.

Results and Discussion

Synthesis. Thioether-amine N_3S ligands L^{N3S} and $L^{N3S'}$ have been previously synthesized and studied by Rorabacher and co-workers[22,24] for ligand−copper ion binding and redox properties. Ligand L^{N3S} or derivatives have also been utilized by Berreau and co-workers[44] for copper(II) complex hydrolytic chemistry and by Zubieta and co-workers[45] for Re/Tc complex studies. The preparation of L^{N3S} used for the present studies was recently published,[35] and that for $L^{N3S'}$ is given in the Experimental Section. The air-sensitive complexes **1-ClO_4**,[35] **1-$B(C_6F_5)_4$**,[35] and **2** were synthesized and handled using standard Schlenk techniques. The structures of **1-$B(C_6F_5)_4$**, as well as a copper(II) complex, **3**, were confirmed by X-ray crystallography (vide infra).

X-ray Crystal Structures. Reaction of L^{N3S} and $[Cu^I(CH_3CN)_4](B(C_6F_5)_4)$ under anaerobic condition in CH_2Cl_2 gives a off-white air-sensitive complex, formulated as **1-$B(C_6F_5)_4$** on the basis of elemental analysis and NMR spectroscopy. Attempts to grow crystals of this complex in CH_2Cl_2/diethylether lead to the isolation of a dinuclear complex, $[\{Cu^I(L^{N3S})\}_2](B(C_6F_5)_4)_2$ (**1-$(B(C_6F_5)_4)_2$**, Figure 4). Crystal data and details of the structure determination for **1-$(B(C_6F_5)_4)_2$**

(43) Brady, L. E.; Freifelder, M.; Stone, G. *J. Org. Chem.* **1961**, *26*, 4757−4758.

(44) Tubbs, K. J.; Fuller, A. L.; Bennett, B.; Arif, A. M.; Berreau, L. M. *Inorg. Chem.* **2003**, *42*, 4790−4791.

(45) Lazarova, N.; Babich, J.; Valliant, J.; Schaffer, P.; James, S.; Zubieta, J. *Inorg. Chem.* **2005**, *44*, 6763−6770.

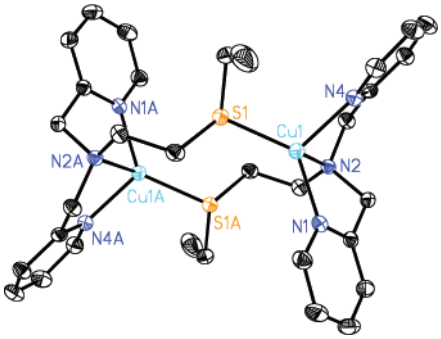

Figure 4. ORTEP diagram of the cationic component of $[\{Cu^{I}(L^{N3S})\}_2](B(C_6F_5)_4)_2$ (**1-(B(C$_6$F$_5$)$_4$)$_2$**). Thermal ellipsoids are drawn by ORTEP and represent 50% probability surfaces.

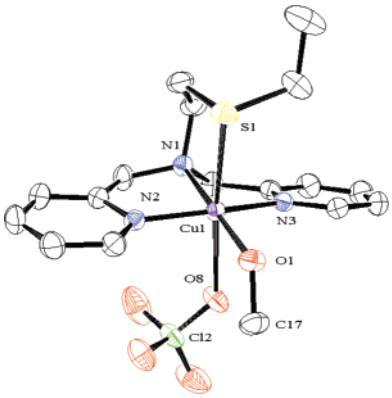

Figure 5. ORTEP diagram of the cationic component of $[Cu^{II}(L^{N3S})(MeOH)](ClO_4)_2$ (**3**). Thermal ellipsoids are drawn by ORTEP and represent 50% probability surfaces.

are provided in Supporting Information (Table S1). Selected bond lengths and bond angles of this complex are listed in Table 1.

Dimer **1-(B(C$_6$F$_5$)$_4$)$_2$** is a centrosymmetric structure (Figure 4), where each copper ion is coordinated by one ligand via the three N-donors and by the other ligand via the thioether atom, thus giving the overall dinuclear structure. Each copper ion shows a pyramidal arrangement of ligands, with the three nitrogens comprising the basal plane and the apical position occupied by one S-atom. Other tetra- or pentacoordinate copper(I) complexes containing at least one thioether ligand exhibit $Cu-S_{thioether}$ bond distances between 2.2 and 2.44 Å.[22,29,32,46−48] Thus, the Cu−S distance of 2.2023 Å in **1-(B(C$_6$F$_5$)$_4$)$_2$** is fairly typical.

Complex **3** adopts a distorted octahedral copper(II) structure (Figure 5) with all three amine ligands and a methanol oxygen atom donor in the equatorial plane. Weak thioether and perchlorate oxygen atom interactions with the copper(II) ion occur via the axial positions with Cu−S = 2.655 Å and Cu−O = 2.57 Å. Table 1 also contains selected bond distance and angle information for **3**. Crystal data and details of the structure determination for **3** are provided in the Supporting Information (Table S2).

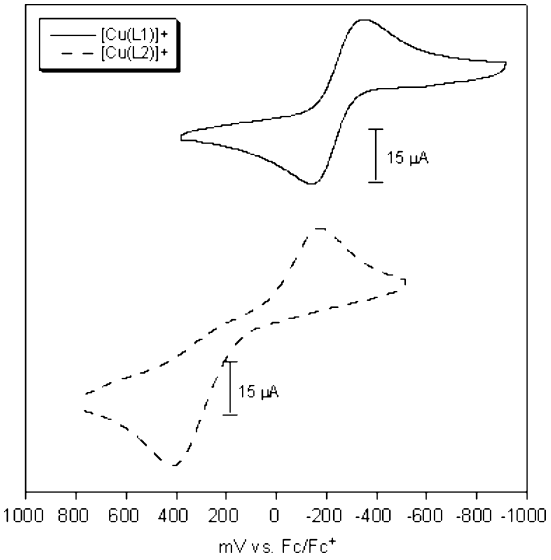

Figure 6. Cyclic voltammograms of **1-ClO$_4$** (top) and **2** (bottom) in acetonitrile.

These Cu(I) and Cu(II) complexes possess certain aspects of the structural features of PHM. Extended X-ray absorption fine structure (EXAFS) spectroscopic studies of PHM and DβH indicate that the $Cu-S_{Met}$ distance is 2.2−2.3 Å for reduced enzyme forms,[49,50] and thus, the Cu−S distance (2.2023 Å) in the present complex **1-(B(C$_6$F$_5$)$_4$)$_2$** is fairly similar. On the other hand, X-ray diffraction studies indicate an oxidized PHM form has the Cu_M site coordinated by two histidine residues and a solvent molecule on the basal plane, with an elongated $Cu-S_{Met}$ bond (or distance) of 2.68 Å.[8] The axial $Cu^{II}-S_{thioether}$ bond in the hexacoordinate structure **3** is elongated Cu^{II} (Cu−S = 2.655 Å), which in fact is typical for related structures, being 2.63−2.94 Å.[25,30,51] For other geometries or lower coordination numbers, Cu(II)−thioether bond lengths fall in the 2.33−2.53 Å range,[28,52−54] where the higher end values arise from highly distorted trigonal bipyramidal structures.[53]

Redox Comparisons. As part of our efforts to evaluate the effects of the thioether ligand on copper complex O_2-reactivity, we measured the redox potentials of **1-ClO$_4$** and **2** by cyclic voltammetry (Figure 6). Both species exhibit quasi-reversible behavior; **2** behaves much more poorly, possessing a very large separation between cathodic and anodic waves, indicating slow electron-transfer kinetics at the electrode surface; however the ratio of current amplitudes (i_{pa}/i_{pc}) is close enough to unity (Figure 6) to consider that a one-electron process occurs. The slow electrode electron-transfer kinetic behavior (for **2**) is a common occurrence for

(46) Karlin, K. D.; Dahlstrom, P. L.; Stanford, M. L.; Zubieta, J. *J. Chem. Soc. Chem. Commun.* **1979**, 465−466.
(47) Karlin, K. D.; Hayes, J. C.; Hutchinson, J. P.; Zubieta, J. *Inorg. Chim. Acta* **1983**, *78*, L45−L46.
(48) Karlin, K. D.; Dahlstrom, P. L.; Hyde, J. R.; Zubieta, J. *J. Chem. Soc. Chem. Commun.* **1980**, 906−908.
(49) Eipper, B. A.; Quon, A. S. W.; Mains, R. E.; Boswell, J. S.; Blackburn, N. J. *Biochemistry* **1995**, *34*, 2857−2865.
(50) Reedy, B. J.; Blackburn, N. J. *J. Am. Chem. Soc.* **1994**, *116*, 1924−1931.
(51) Prochaska, H. J.; Schwindinger, W. F.; Schwartz, M.; Burk, M. J.; Bernarducci, E.; Lalancette, R. a.; Potenza, J. a.; Schugar, H. J. *J. Am. Chem. Soc.* **1981**, *103*, 3446−3455.
(52) Ruf, M.; Pierpont, C. G. *Angew. Chem., Int. Ed.* **1998**, *37*, 1736−1739.
(53) Otsuka, M.; Hamasaki, A.; Kurosaki, H.; Goto, M. *J. Organomet. Chem.* **2000**, *611*, 577−585.
(54) Klein, E. L.; Khan, M. A.; Houser, R. P. *Inorg. Chem.* **2004**, *43*, 7272−7274.

Table 1. Selected Bond Distances and Angles for $[\{Cu^{I}(L^{N3S})\}_2](B(C_6F_5)_4)_2$ (**1-$(B(C_6F_5)_4)_2$**) and $[Cu^{II}(L^{N3S})(MeOH)](ClO_4)_2$ (**3**)

		1-$(B(C_6F_5)_4)_2$		**3**
		Bond Lengths (Å)		
Cu−S	Cu(1)−S(1)	2.2023(9)	Cu(1)−S(1)	2.6551 (7)
$Cu-N_{amine}$	Cu(1)−N(2)	2.2556(18)	Cu(1)−N(1)	2.0302 (19)
$Cu-N_{py}$	Cu(1)−N(1)	2.0158(18)	Cu(1)−N(2)	1.981 (2)
	Cu(1)−N(4)	2.0646(19)	Cu(1)−N(3	1.983 (2)
Cu−O			Cu(1)−O(1)	2.0009 (17)
			Cu(1)−O(8)	2.57
		Bond Angles (deg)		
	N(1)−Cu(1)−N(4)	115.52(7)	N(2)−Cu(1)−N(3)	164.01 (8)
	N(1)−Cu(1)−S(1)	129.81(6)	N(2)−Cu(1)−O(1)	96.36 (8)
	N(4)−Cu(1)−S(1)	112.82(6)	N(3)−Cu(1)−O(1)	96.93 (8)
	N(1)−Cu(1)−N(2)	80.80(7)	N(2)−Cu(1)−N(1)	84.41 (8)
	N(4)−Cu(1)−N(2)	78.62(7)	N(3)−Cu(1)−N(1)	82.20 (8)
	S(1)−Cu(1)−N(2)	121.88(5)	N(2)−Cu(1)−O(8)	94.0
			O(1)−Cu(1)−N(1)	178.94 (8)
			N(2)−Cu(1)−S(1)	90.00 (6)
			N(3)−Cu(1)−S(1)	98.11 (6)
			O(1)−Cu(1)−S(1)	93.13 (6)
			N(1)−Cu(1)−S(1)	87.61 (6)
			O(8)−Cu(1)−S(1)	175.6

Table 2. Cu^{II}/Cu^{I} Redox Potential ($E_{1/2}$) Values Measured on Copper(I) Complexes[a]

N_3S ligand complexes	$E_{1/2}$ vs $Fe(cp)_2^{+/0}$	N_4 ligand complexes	$E_{1/2}$ vs $Fe(cp)_2^{+/0}$
$[Cu^{I}(L^{N3S})]^+$	−0.25 V	$[Cu^{I}(TMPA)(MeCN)]^+$	−0.40 V
$[Cu^{I}(L^{N3S'})]^+$	−0.12 V	$[Cu^{I}(PMAP)]^+$	−0.25 V

[a] Acetonitrile solvent.

tripodal tetradentate ligand copper complexes with six-membered chelate rings.[33] The complex containing the "short armed" ligand (**1-ClO_4**) exhibits an $E_{1/2}$ value which is ~0.37 V more negative than that for **2**, Table 2. As both L^{N3S} and $L^{N3S'}$ are close analogues to complexes with TMPA and PMAP ligands, whereby one pyridyl arm is substituted by a CH_2CH_2-S-Et group (Figure 3), it is worthwhile to compare copper(I) complex redox potentials. In acetonitrile, $[Cu^{I}(TMPA)(MeCN)]^+$ has a Cu^{II}/Cu^{I} redox potential of −0.40 V vs $Fe(cp)_2^{+/0}$ while that for $[Cu^{I}(PMAP)]^+$ is −0.25 V (Table 2).[55] Hence, the thioether donor in **1** raises the redox potential by 0.15 V in comparison to the copper(I) complex of TMPA having only amine donors; similarly **2** has an $E_{1/2}$ which is 0.13 V higher than that for the analogous $[Cu(PMAP)]^+$ complex (Table 2).

Thus, these studies confirm two facets of previously known factors that raise the redox potentials of copper(I) complexes, the thioether donor and the Cu-chelate ring size of six. The latter trend was observed in a number of individual studies,[33,56−59] and has been examined and analyzed by Rorabacher and co-workers.[22,24] The effect has been shown to arise from the differences in the formation constants of the ligand−Cu^{II} complexes (from copper(II) ion and free ligand) of a five- versus a six-membered ligand chelate ring; binding of the five-membered ring chelate ligand to copper(II) is thermodynamically favored. By contrast, formation constants for the corresponding ligand−Cu^{I} species are generally unaffected by the chelate ring size or donor atom.

Carbon Monoxide Binding. As another means of comparing complexes **1** and **2** with the corresponding amine-ligand counterparts, we measured the C−O stretching frequencies for the respective carbonyl adducts. The preparation of **1-CO** was performed in situ by bubbling excess CO(g) into a dichloromethane or acetonitrile solution of **1-ClO_4** (eq 1). Interestingly, the same preparation was unsuccessful for generating an analogue $[Cu^{I}(L^{N3S'})(CO)]^+$ (**2-CO**), indicating a distinct difference between **1** and **2** in the ability to bind CO (eqs 1 and 2). The $[Cu^{I}(PMAP)]^+$ amine analogue, however, does react with CO and forms a carbonyl adduct $[Cu^{I}(PMAP)(CO)]^+$ ($\nu(C-O) = 2090\ cm^{-1}$),[55] indicating that the sulfur ligation is influencing the CO binding ability of **2**.

$$[Cu(L^{N3S})]^+ + CO(g) \rightarrow [Cu(L^{N3S})(CO)]^+ \quad (1)$$

$$[Cu(L^{N3S'})]+ + CO(g) \rightarrow \text{No Reaction} \quad (2)$$

The solution (acetonitrile) IR spectrum of $[Cu^{I}(TMPA)(CO)]^+$ exhibits two $\nu(C-O)$ stretching frequencies at 2092 and 2077 cm^{-1}, which has been previously attributed to a dynamic equilibrium involving a pyridyl arm binding or coming off of the copper(I) ion.[5,55,60] The 2092 cm^{-1} peak has been assigned as the $[Cu^{I}(TMPA)(CO)]^+$ complex wherein only three amine ligands of the TMPA ligand coordinated, and the lower energy peak is assigned as the $[Cu^{I}(TMPA)(CO)]^+$ complex with all four amine ligands coordinated to the copper(I).[5,55,60] The IR spectrum of a solution of in situ generated **1-CO** exhibits a sharp carbonyl vibration at 2094 cm^{-1} in acetonitrile and 2096 cm^{-1} in dichloromethane. Because these values are almost identical to those of $[Cu^{I}(TMPA)(CO)]^+$, where the TMPA provides tridentate coordination, we propose that L^{N3S} behaves as a

(55) Fry, H. C. Ph.D. Dissertation, Johns Hopkins University, 2004.
(56) Nikles, D. E.; Powers, M. J.; Urbach, F. L. *Inorg. Chem.* **1983**, *22*, 3210−3217.
(57) Karlin, K. D.; Yandell, J. K. *Inorg. Chem.* **1984**, *23*, 1184−1188.
(58) Karlin, K. D.; Sherman, S. E. *Inorg. Chim. Acta* **1982**, *65*, L39−L40.
(59) Karlin, K. D.; Hayes, J. C.; Shi, J.; Hutchinson, J. P.; Zubieta, J. *Inorg. Chem.* **1982**, *21*, 4106−4108.
(60) Kretzer, R. M.; Ghiladi, R. A.; Lebeau, E. L.; Liang, H.-C.; Karlin, K. D. *Inorg. Chem.* **2003**, *42*, 3016−3025.

"tridentate" ligand in the presence of CO in solution, with the thioether not coordinated (see diagram).[61]

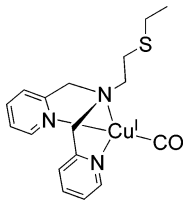

This makes the three amine ligands of L^{N3S} creating a copper(I) environment equivalent to that of $[Cu^{I}(TMPA)(CO)]^{+}$. Overall tetra- compared to pentacoordination for copper(I) is generally preferred and this coordination property contributes to the lack of thioether ligation in **1-CO**. However, the thioether S-atom is thought to coordinate and influence the properties of the O_2-adduct of **1**, as described below.

Copper−Dioxygen Reactivity of 1. While the "short arm" $[Cu^{I}(TMPA)(MeCN)]^{+}$ complex forms a low-temperature stable "end-on" μ-1,2-peroxodicopper(II) species $[\{Cu^{II}(TMPA)\}_2(\mu\text{-}1,2\text{-}O_2^{2-})]^{2+}$ (**5**) (diagram),[5,6] the "long arm"

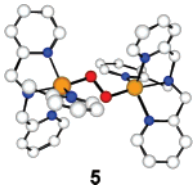

5

amine complex $[Cu^{I}(PMAP)]^{+}$ (Figure 3) does not react with O_2 at low temperature, presumably due to the fact that the $Cu^{II/I}$ redox potential is considerably more positive than that for $[Cu^{I}(TMPA)(MeCN)]^{+}$.[33] Interestingly, **1-ClO$_4$** exhibits essentially the same redox potential as $[Cu^{I}(PMAP)]^{+}$ (−0.25 V vs $Fe(cp)_2^{+/0}$, Table 2), yet it does react with O_2 and forms what we formulate as an end-on peroxo complex, **4** (Scheme 1),[62] as observed by UV−vis and rR spectroscopy (vide infra).

Scheme 1

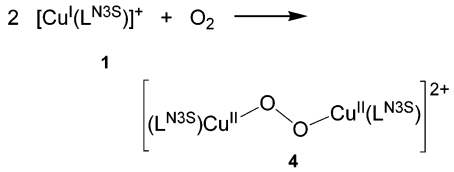

At −80 °C, reaction of **1-ClO$_4$** with O_2 in CH_2Cl_2, acetone, or 2-methyltetrahydrofuran (MeTHF) results in a rapid change to a dark blue solution. The solution color persists for only 10−20 min and slowly decompose to a green species. However, oxygenation of **1-B(C_6F_5)$_4$**, instead of **1-ClO$_4$**, under colder conditions (−125 °C in MeTHF) leads

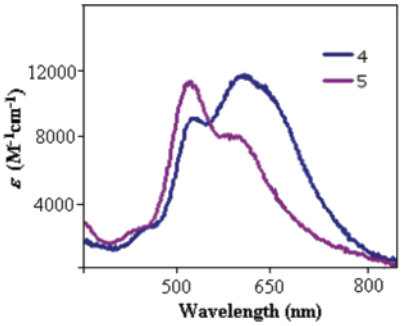

Figure 7. Absorbance spectra of μ-1,2-peroxodicopper(II) complexes $[\{Cu^{II}(TMPA)\}_2(\mu\text{-}1,2\text{-}O_2^{2-})]^{2+}$ (**5**, purple) with N_4 TMPA ligand, and **4** (blue) with thioether N_3S ligand L^{N3S}.

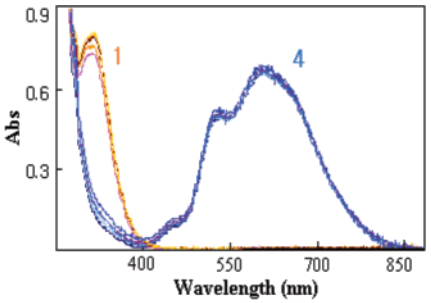

Figure 8. UV−vis spectra demonstrating the reversible O_2-binding behavior of $[Cu^{I}(L^{N3S})]^{+}$ (**1-B(C_6F_5)$_4$**) in Me-THF. A colorless solution of **1** (λ_{max} = 340 nm, spectrum **1**) bubbled with O_2 (at −127 °C) leads to the dark blue dioxygen adduct $[\{(L^{N3S})Cu^{II}\}_2(\mu\text{-}1,2\text{-}O_2^{2-})]^{2+}$ (**4**) (λ_{max} = 605 nm, spectrum **4**). Application of a vacuum while warming to −90 °C leads to solution decoloration and **1** is cleanly regenerated (O_2 dissociation as monitored by UV−vis spectroscopy is observable even at −127 °C but it occurs very slowly). Four cycles are shown, and these are virtually overlapped; thus, there appears to be no detectable decomposition.

to formation of a stable species (Figure 7, blue spectrum); the new dioxygen adduct, formulated as a μ-1,2-peroxodicopper(II) complex **4** (see the following section), has absorption transitions with similar energies and total intensities to those of **5** with λ_{max} = 530 ($\epsilon \approx 9200$ M^{-1} cm^{-1}) and 605 nm ($\epsilon \approx 11\,800$ M^{-1} cm^{-1}) (Figure 7). The binding of O_2 to **1-B(C_6F_5)$_4$** is reversible, as evidenced by reactions interconverting complexes **1-B(C_6F_5)$_4$** and **4** (Figure 8).

One notable feature in the absorbance spectrum of **4** is that the 16 560 cm^{-1} (604 nm) band is more intense than the 18 870 cm^{-1} (530 nm) band, which is opposite to that observed for $[\{Cu^{II}(TMPA)\}_2(\mu\text{-}1,2\text{-}O_2^{2-})]^{2+}$ and other end-on peroxo dicopper(II) complexes.[1−4,63−66] While the thioether S-donor in the N_3S donor set of L^{N3S} is not coordinated in the $[Cu(L^{N3S})(CO)]^{+}$ complex (vida supra), the UV−vis characteristics suggest that it is coordinated to the copper(II) ion in the end-on peroxo species **4**. If it were not, then the remaining "tridentate amine" ligand (N_3 portion of L^{N3S}) would, according to precedent, likely form a very unstable bis-μ-oxo complex ($\lambda_{max} \approx 385$ nm).[67] EXAFS studies

(61) Supporting evidence (unpublished) comes from our observation that when a copper(I)−ligand analogue of L^{N3S} where the ligand does not possess the $-CH_2CH_2SEt$ arm, but a benzyl or methyl group instead (i.e., thus with just N_3 ligation), the CO stretching frequency also comes at 2093 cm^{-1}.

(62) Hatcher, L. Q.; Vance, M. A.; Narducci Sarjeant, A. A.; Solomon, E. I.; Karlin, K. D. *Inorg. Chem.* **2006**, *45*, 3004−3013.

(63) Henson, M. J.; Vance, M. A.; Zhang, C. X.; Liang, H.-C.; Karlin, K. D.; Solomon, E. I. *J. Am. Chem. Soc.* **2003**, *125*, 5186−5192.

(64) Komiyama, K.; Furutachi, H.; Nagatomo, S.; Hashimoto, A.; Hayashi, H.; Fujinami, S.; Suzuki, M.; Kitagawa, T. *Bull. Chem. Soc. Jap.* **2004**, *77*, 59−72.

(65) Becker, M.; Heinemann, F. W.; Schindler, S. *Chem. Eur. J.* **1999**, *5*, 3124−3129.

(66) Bol, J. E.; Driessen, W.; Ho, R. Y. N.; Maase, B.; Que, J., L.; Reedijk, J. *Angew. Chem., Int. Ed. Engl.* **1997**, *36*, 998−1000.

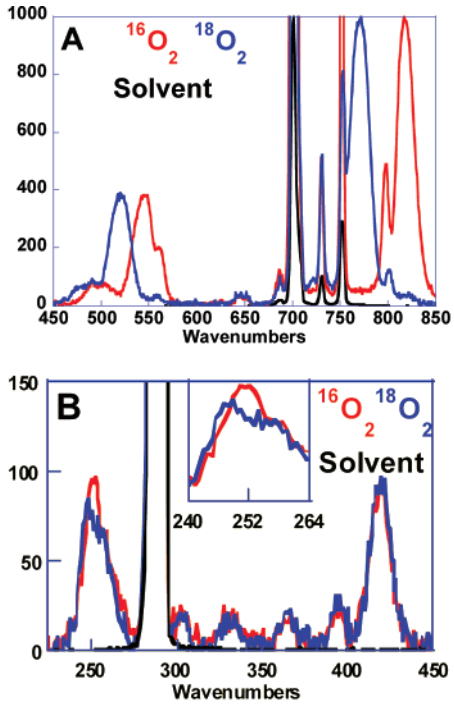

Figure 9. rR spectra of $[\{Cu^{II}(L^{N3S})\}_2(\mu\text{-}1,2\text{-}O_2^{2-})]^{2+}$ (**4**) in CH_2Cl_2 (λ_{ex} = 620 nm) with $^{16}O_2$ (in **red**) and $^{18}O_2$ (in blue) isotopic substitution. Solvent peaks are overlaid in black. Inset of **B**: Blow-up of the 250 cm^{-1} peak and isotope shifting observed. See text for further description.

confirm thioether ligation in **4** (vide infra). The origin of the atypical absorption spectrum was further investigated by rR spectroscopy.

Resonance Raman Spectroscopy of 4. As described in our preliminary communication,[35] rR spectra of **4** in CH_2Cl_2 with $^{16}O_2$ and $^{18}O_2$ isotopic substitution were collected with 620 nm excitation. The primary features were the ν(O−O) band at 817 cm^{-1} ($^{18}O_2$ Δ = −46 cm^{-1}) and the symmetric ν(Cu−O) vibration at 545 cm^{-1} ($^{18}O_2$ Δ = −26 cm^{-1}; Figure 9A).[68] These values are similar to those previously observed for **5**[69] {ν(O−O) = 827 cm^{-1} and ν_{sym}-(Cu−O) = 561 cm^{-1}} and allow the assignment of **4** as an end-on peroxide-bridged structure.[1−3] The lower (compared to **5**) vibrational frequencies indicate that O−O and Cu−O bonding is weaker overall in **4** than in the TMPA complex; the lower ν(Cu−O) frequency indicates less electron-donation to copper from the peroxide π* orbital, which in turn also weakens the O−O bond (i.e., more electron density in the O−O antibonding orbital) and lowers ν(O−O) as well. As discussed below, these effects can be ascribed to thioether (instead of pyridyl nitrogen) ligation in **4**.

Additional broad and weak vibrational features at ∼500 cm^{-1} (Figure 9A) also shift with dioxygen isotopic substitution. The magnitude of the shift is not clear due to overlap with the ν_{sym}(Cu−O) mode and possible Fermi interactions,

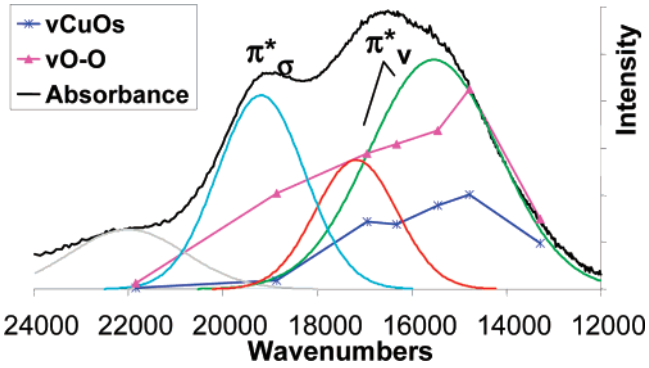

Figure 10. rR profile of ν(O−O) (pink triangles) and ν(Cu−O) (blue stars) of $[\{Cu^{II}(L^{N3S})\}_2(\mu\text{-}1,2\text{-}O_2^{2-})]^{2+}$ (**4**) in CH_2Cl_2. The absorbance spectrum (black) and Gaussian fit transitions (gray, cyan, red, and green) are also shown. See text for further discussion and explanation.

but it is in the expected range for the antisymmetric ν(Cu−O) mode.[63,69] There is another isotope-sensitive vibration at ∼250 cm^{-1} ($^{16-18}O_2$ Δ = ∼4 cm^{-1}; Figure 9B). This is likely a bending motion with Cu−O character. The remaining resonance enhanced modes show no $^{18}O_2$ isotope shift and are thus associated with the Cu−N ligands. The 419 cm^{-1} vibration (Figure 9B) has been assigned as the ν(Cu−N) mode of the tertiary amine.[63,69] Additional weak features at ∼393, 365, 330, 305, and 263 cm^{-1} are likely (Cu−N)/(Cu−S) stretching and bending or other internal ligand modes (Figure 9B).

To investigate for the possible presence of a thioether-to-Cu LMCT, the broad visible absorption feature was profiled between 458 and 752 nm (∼22 000 and ∼13 000 cm^{-1}) by rR spectroscopy (Figure 10).[70] The ν(O−O) mode profiles weakly across the ∼19 200 cm^{-1} transition (Figure 10, cyan), strongly in the ∼15 500 cm^{-1} transition (Figure 10, green), and not at all at ∼22 000 cm^{-1} (Figure 10, gray); ν(Cu−O)$_S$ shows almost no resonance intensity at ∼19 200 cm^{-1}, but has strong enhancement in the ∼15 500 cm^{-1} transition (Figure 10, green) and no enhancement at ∼22 000 cm^{-1}.[63,70] These enhancement patterns are similar to those observed in $[\{Cu^{II}(TMPA)\}_2(\mu\text{-}1,2\text{-}O_2^{2-})]^{2+}$,[69] allowing assignment of the ∼15 500 cm^{-1} transition (Figure 10, green) as a π^*_v-to-Cu charge transfer, the ∼19 200 cm^{-1} transition (Figure 10, cyan) as a π^*_σ-to-Cu charge transfer, and the ∼22 000 cm^{-1} band (Figure 10, gray) as the spin-forbidden triplet charge-transfer transition from the π^*_v orbital. These three transitions alone are not sufficient for a good Gaussian fit of the absorbance spectrum. Another band is needed, and both the ν(Cu−O) and ν(O−O) profiles exhibit a shoulder at ∼17 200 cm^{-1} (Figure 10, red). Given that the ∼17200 cm^{-1} shoulder shows ν(Cu−O)$_S$ mode enhancement similar to that observed in the ∼15,500 cm^{-1} band (Figure 10, green), this shoulder is assigned as a second π^*_v-to-Cu charge-transfer transition. Other rR peaks show much weaker enhancement. Importantly, no modes show enhancement consistent with the presence of a S−Cu stretch, which would be associated with a thioether-to-Cu(II) CT transition. Thus, the thioether-to-

(67) Osako, T.; Ueno, Y.; Tachi, Y.; Itoh, S. *Inorg. Chem.* **2003**, *42*, 8087−8097.
(68) We here note that the $^{16}O_2$ derived features were slightly split (with additional peaks at ∼800 and ∼560 cm^{-1}) which gain some intensity through Fermi mixing; they were not present in the $^{18}O_2$ prepared sample.
(69) Baldwin, M. J.; Ross, P. K.; Pate, J. E.; Tyeklár, Z.; Karlin, K. D.; Solomon, E. I. *J. Am. Chem. Soc.* **1991**, *113*, 8671−8679.
(70) The possibility of multiple species being present was dismissed after inspection of the ν(O-O) stretch overlaid across the laser lines profiled. The peak shape did not change over the profile, so the sample is likely composed of just one end-on peroxo species.

Cu(II) CT transition must be at >30 000 cm^{-1} as is observed in other Cu(II) complexes.[48,53,56,71,72]

As described above, there are significant absorption spectral differences between **4** and **5** which can provide insight into structure. First, the relative intensities of the π^*_σ/π^*_v transitions are reversed in **4** relative to the TMPA complex with the π^*_v transition being more intense in **4** (Figure 10). This indicates that the π^*_v orbital has more overlap with the half-occupied orbital on the Cu(II) than in the TMPA complex, supporting the assertion of a distorted ligand field around the Cu center. The π^*_σ orbital is, however, at a deeper energy as it is involved in σ bonding with the Cu. Although the position of the π^*_σ charge-transfer band remains essentially unchanged, the lower intensity indicates that it has less overlap with the half-occupied orbital on the Cu(II). The more intense π^*_v transition has shifted to lower energy, indicating weaker π^*_v bonding and weaker Cu−O bonding overall. This is consistent with the observed rR data.

Another notable spectral difference between **4** and **5** is the ∼17 000 cm^{-1} splitting of the π^*_v transition into two components, which is similar in magnitude to the charge-transfer splitting observed in other bridged copper complexes.[73] Assuming at least C_2 symmetry in the Cu_2O_2 unit, the π^*_v CT state would be split by interaction of the charge-transfer transitions to the two Cu(II) into A and B components with the B component being at lower energy.[74,75] This allows assignment of the ∼15 500 cm^{-1} band as a π^*_v -to-Cu (B) transition and the ∼17 200 cm^{-1} band as a π^*_v -to-Cu (A) transition. The two π^*_σ-to-Cu(II) charge-transfer transitions would also couple to form two split states in the bridged dimer. However, because excited-state splitting is derived from ligand overlap with the half-occupied metal d-orbitals and the π^*_σ transition is less intense, a smaller splitting would be expected and is not observed.

Application of a transition dipole-vector coupling model to the intensity distribution of the π^*_v transitions can provide insight into the degree of distortion of the Cu_2O_2 unit.[74] The integrated intensity ratio of the π^*_v transitions (I_A/I_B = ∼0.36) relates to the angle between the transition dipoles and the C_2 axis, which is calculated to be ∼60° for **4**. This indicates a high degree of Cu_2O_2 core distortion, likely an out-of-plane bend, compared to the nearly planar Cu_2O_2 found in the TMPA complex, which has intensity in only one component of the π^*_v charge transfer (indicating that the monomer dipoles are both perpendicular (90°) to the C_2 axis). This distortion is likely due to steric effects. **5** and $[Cu^{II}(TMPA)Cl]^+$ maintain a trigonal bipyramidal geometry.[5,59] However, other complexes with tripodal tetradentate ligands having (i) six-substituted pyridyl arms,[76] (ii) lengthened arms,[59,77] or (iii) an arm with thioether instead of a methylpyridyl,[46] including **3** (vide supra), are distorted toward a square pyramidal geometry with the modified ligand at the apex of the pyramid to minimize steric interaction with the fifth ligand (here dioxygen). This distortion leads to decreased π^*_σ overlap, greater π^*_v overlap, and a weakened Cu−O bond.

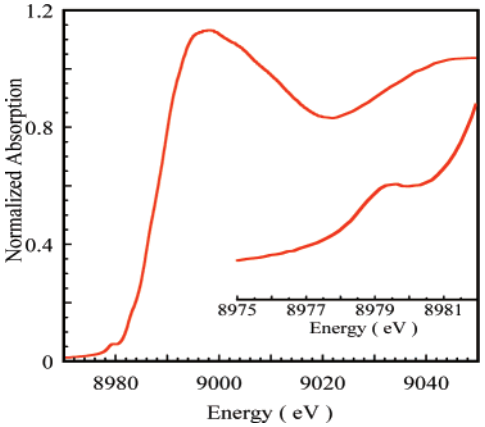

Figure 11. Normalized Cu K-edge XAS spectrum of **4**. Inset shows the expanded pre-edge region and the 1s→3d transition at ∼8979 eV.

EXAFS Spectroscopy. The most compelling evidence for the presence of thioether ligation in **4** is the EXAFS spectrum, obtained from frozen (MeTHF) solution. The results were described in our preliminary communication.[35] A more detailed analysis of the Cu K-edge and EXAFS data of **4** is presented here. A comparison of the EXAFS data of **4** is made with that of the decomposition product.

Cu K-Edge. The normalized X-ray absorption Cu K-edge and pre-edge (as inset) spectra of **4** are shown in Figure 11. These data have been analyzed to estimate the conversion of the Cu(I) starting material to the end-on Cu_2O_2 dimer. The pre-edge feature observed at ∼8979 eV is characteristic of a Cu(II) complex and corresponds to the electric dipole-forbidden quadrupole-allowed 1s→3d transition.[78] The presence of this feature indicates that **4** contains significant Cu(II) character. The XAS spectra of a Cu(I) species display an intense feature at ∼8984 eV which is assigned to the dipole allowed 1s→4p transition.[79] Comparison of the Cu K-edge data of **4** with XAS spectral simulations of several Cu(II) complexes with different amounts of Cu(I) contamination indicate that **4** contains <5% of the unconverted Cu(I) species.

EXAFS. The k^3-weighted Cu K-edge EXAFS data and their Fourier transforms (FT) for **4** are presented in Figure S3. The EXAFS fit parameters are given in Table S1. The first shell EXAFS was fit with 1 Cu−O/N contribution at

(71) Whittaker, M. M.; Chuang, Y. Y.; Whittaker, J. W. *J. Am. Chem. Soc.* **1993**, *115*, 10029−10035.
(72) Huys, C. T.; Hoste, S.; Goeminne, A. M.; Vanderkelen, G. P. *Spectrochim. Acta A* **1983**, *39*, 631−633.
(73) Tuczek, F.; Solomon, E. I. *Inorg. Chem.* **1993**, *32*, 2850−2862.
(74) Eickman, N. C.; Himmelwright, R. S.; Solomon, E. I. *Proc. Natl. Acad. Sci. U.S.A.* **1979**, *76*, 2094−2098.
(75) Westre, T. E.; Di Cicco, A.; Fillipponi, A.; Natoli, C. R.; Hedman, B.; Solomon, E. I.; Hodgson, K. O. *J. Am. Chem. Soc.* **1994**, *116*, 6757−6768.
(76) Lucchese, B.; Humphreys, K. J.; Lee, D.-H.; Incarvito, C. D.; Sommer, R. D.; Rheingold, A. L.; Karlin, K. D. *Inorg. Chem.* **2004**, *43*, 5987−5998.
(77) Wei, N.; Murthy, N. N.; Karlin, K. D. *Inorg. Chem.* **1994**, *33*, 6093−6100.
(78) Shulman, R. G.; Yafet, Y.; Eisenberger, P.; Blumberg, W. E. *Proc. Nat. Acad. Sci., U.S.A.* **1976**, *73*, 1384−1388.
(79) Kau, L.-S.; Spira-Solomon, A. J.; Penner-Hahn, J. E.; Hodgson, K. O.; Solomon, E. I. *J. Am. Chem. Soc.* **1987**, *109*, 6433−6442.

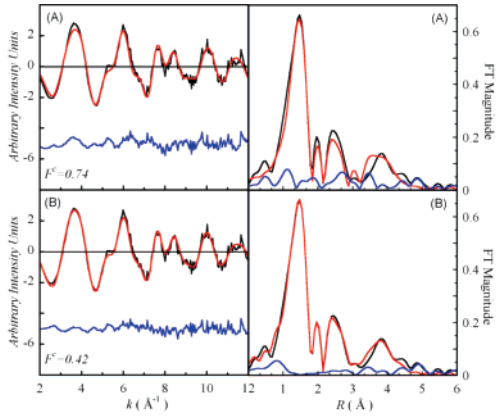

Figure 12. Cu K-edge EXAFS data (left panels) and non-phase-shift-corrected Fourier transforms (right panels). Panels (A) and (B) give fits with a long Cu−O and a Cu−S contribution, respectively. A lower reduced χ^2 error (F^C) reflects a better fit. Data (black), fit (red), and residual (blue).

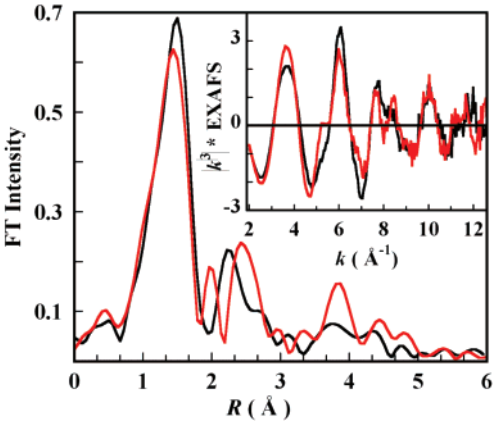

Figure 13. Cu K-edge EXAFS data (inset) and non-phase-shift-corrected Fourier transform of **4** (red) and the temperature-induced decay product (black).

1.89 Å, 3 Cu−N/O at 2.03 Å, and 1 Cu−S at 2.41 Å. The FT shows intense peaks in the R = 2−3 and 3.5−4.5 Å ranges, indicating strong contribution from the L^{N3S} ligand. These second and third shell contributions were fit using single scattering (SS) and multiple scattering (MS) contributions from the L^{N3S} ligand pyridine rings (Table S3). The first shell Cu−S contribution at 2.41 Å was required to obtain a good fit. Replacement of the Cu−S path by single or multiple Cu−O or Cu−C paths resulted in worse fits to the data and clearly indicated a residual in the fits to the EXAFS data. A comparison of the best fit with a long Cu−O path (2.62 Å, in Panel A) and Cu−S path (2.41 Å, in Panel B) is shown in Figure 12.

The edge data for **4** indicate that essentially no unconverted Cu(I) is present. However, **4** is extremely temperature sensitive and could arguably decay to a Cu(II) complex which could contain a Cu−S interaction at ∼2.4 Å. To evaluate this possibility, Cu K-edge EXAFS data were collected on a sample cell containing **4** which had been allowed to warm up to room temperature for ∼2 h. The EXAFS data and Fourier transforms of this decay product are compared to those of **4** in Figure 13. The EXAFS data are clearly different, and this is also manifested in differences in the Fourier transform data. In particular, the peak at ∼2.0 Å in the non-phase-shift-corrected data of **4** is missing in the decay product. Since the calculated phase shift is ∼0.4 Å, this difference in the EXAFS is indicative of the absence of the Cu−S bond in the decay product. The MS contribution from the L^{N3S} ligand system at ∼3.8 Å is also smaller in the decay product, likely indicating a more disordered site compared to **4**. The k^3-weighted Cu K-edge EXAFS data, and their FTs of the decay product are presented in Figure S4. The EXAFS fit parameters are given in Table S4. The first shell EXAFS data were fit with 4 Cu−O/N contributions at 2.0 Å and a long Cu−O at 2.55 Å. The second and third shell components are similar to those of **4** but have higher Debye−Waller factors indicating an increase in disorder. The first shell analysis of the decay product clearly indicates that the Cu−S bond observed in the EXAFS analysis of **4** is only present in the end-on Cu_2O_2 species.

L^{N3S} Chemistry: Modeling DBH and PHM. In contrast to tyrosinase or catechol oxidase, which involve a magnetically coupled dicopper(II) side-on peroxo species as the electrophilic oxidant,[80] the non-coupled binuclear nature of the PHM and DβH active sites (i.e., 11 Å distance between Cu_M and Cu_H in PHM, Figure 1) directs the chemistry to occur at only one mononuclear active site while still providing another reducing electron from a distant Cu^I ion.[15] What is the role of the thioether donor at the mononuclear Cu_M active site? Recent results from our laboratories suggest that a Cu^I complex $[Cu^I(Me_2N\text{-}TMPA)]^+$ having strong amine donors (by way of added dimethylamino electron donor 4-pyridyl substituents on TMPA) can better stabilize a mononuclear superoxo species $[Cu^{II}(NMe_2\text{-}TMPA)(O_2^-)]^+$ as compared to the unsubstituted $[Cu^I(TMPA)]^+$ complex.[81] The $Cu^{II}-(O_2^-)$ moiety forms faster (larger k_{on} in the Cu^I/O_2 reaction) and is thermodynamically more stable (larger $K_{formation}$), and the reverse reaction involving Cu−O bond-breaking (in $[Cu^{II}(NMe_2\text{-}TMPA)(O_2^-)]^+$) possesses a larger activation enthalpy.[34] The corresponding end-on peroxo species, $[\{Cu^{II}(NMe_2\text{-}TMPA)\}_2(O_2^{2-})]^{2+}$, also has a weakened bond, ν(O−O) = 813 cm^{-1}, similar to that of **4**.[63] The result presented here, that the thioether group of L^{N3S} may act as a relatively stronger donor ligand in **4** (vide supra), suggests that the methionine sulfur ligand at Cu_M in DβH and PHM could well facilitate both kinetic and thermodynamic stabilization of a Cu^{II}_M−superoxo intermediate, the active species thought to effect substrate hydrogen-atom abstraction (see Introduction). Chen and Solomon[12] also point out that the Cu_M Met ligand contributes to the stabilization of the Cu^{II}−oxyl species produced later (following O−O bond cleavage) in the reaction mechanism (Figure 1, bottom left).

Ligand Substrate Reactivity of 4. The room-temperature O_2-reactivity of **1** is also noteworthy giving further insight into Cu−dioxygen bonding and reactivity in the presence of a thioether ligand; complex **1-ClO$_4$** exhibits copper-

(80) Solomon, E. I.; Sundaram, U. M.; Machonkin, T. E. *Chem. Rev.* **1996**, *96*, 2563−2605.
(81) Maiti, D.; Fry, H. C.; Woertink, J. S.; Vance, M. A.; Solomon, E. I.; Karlin, K. D. *J. Am. Chem. Soc.* **2007**, *129*, 264−265.

Scheme 2

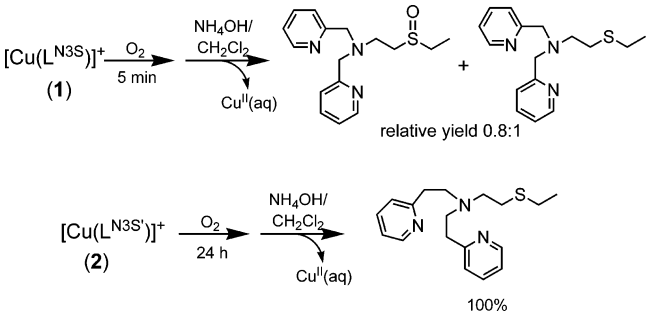

Scheme 3

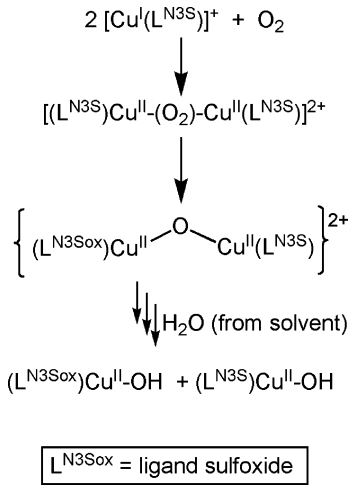

mediated oxygen atom transfer to the ligand in high yields. Upon addition of O_2 to **1-ClO$_4$** in CH_2Cl_2, the solution quickly turns aqua/blue. After demetallation with NH_4OH-(aq), analysis of the recovered ligand showed that 44% of the thioether-amine ligand was oxidized to the sulfoxide derivative (L^{N3Sox}) (according to ^1H NMR and high-resolution MS, see Experimental Section), Scheme 2.

As observed in other chemical systems,[4,82−84] a 50% yield is all that is expected for a monooxygenase model system where a four-electron reduction of O_2 is accomplished with (formally) one oxygen atom derived from the O_2 molecule being incorporated into a substrate and where the other O-atom is reduced to the oxidation state level of water. In the monooxygenase reaction of **1**, as two electrons are needed from the two copper(I) ions, only one of the ligands on one copper can become oxidized and the theoretical maximum is a 50% yield (Scheme 3).

We find that when the reaction is carried out using labeled $^{18}O_2$, ^{18}O is incorporated into the sulfoxide ligand to the extent of 58%, a relatively low level of oxygen atom incorporation, but still indicating the sulfoxide O-atom derives from O_2 and a copper−dioxygen species. Also consistent with this result is the finding that a sulfoxidation

Scheme 4

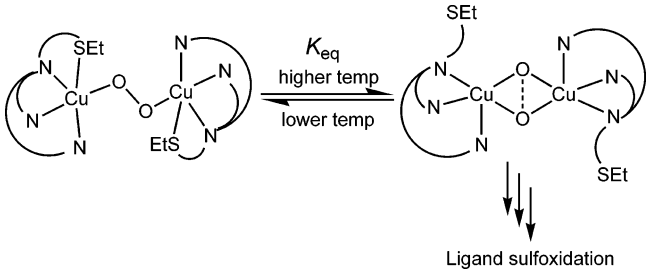

reaction occurs from the reaction of **3** with 10 equiv of H_2O_2 (eq 3). In this "peroxide shunt" reaction, we observe 74% ligand oxidation. Sulfoxidation reactions mediated by Cu^{II} and H_2O_2 are not uncommon.[29,30]

$$(L^{N3S})Cu^{II} + H_2O_2 \rightarrow (L^{N3Sox})Cu^{II} + H_2O \qquad (3)$$

It has been previously established that, for the most part, end-on peroxo dicopper(II) compounds are nucleophilic or basic by their nature.[85,86] They react with PPh_3 displacing O_2 and subsequently form $Cu^I(PPh_3)$ moieties; they also protonate releasing H_2O_2.[85,86] By contrast, side-on peroxo dicopper and bis(μ-oxo) isomer species are known to be electrophilic, carrying out ligand or substrate oxygen atom transfer or oxidation (e.g., H-atom abstraction) reactions.[4,85,86] Thus, to account for the sulfoxidation of L^{N3S} via formation of **4**, we suggest that it may be a side-on μ-η^2:η^2 peroxodicopper or bis-μ-oxo dicopper(III) isomer form which could be in equilibrium with the end-on peroxo complex **4** and which effects the oxygen-atom transfer reaction (Scheme 4). Such equilibrium mixtures are known.[87,88] The end-on peroxo structure **4** equilibrium form would be favored at low temperature, in line with the UV−vis and rR spectroscopic properties (vide supra). However, warming would perhaps favor a N_3-ligated-thioether dangling form (Scheme 4), wherein intramolecular attack of the thioether substrate then occurs. This hypothesis could also account for the observation that prolonged standing of **4** at low temperature (−80 °C), even followed by warming, results in significantly reduced yields (<25%) of sulfoxide. We should also note that Itoh and co-workers[89] have demonstrated bis-μ-oxodicopper(III) sulfoxidation of exogenously added (but also demonstrated to bind to copper) thioether substrates.

Lack of Copper−Dioxygen Reactivity with 2. In contrast to the oxidative chemistry observed for the copper complexes of the "short arm" L^{N3S}, complex **2** does not react with dioxygen. Addition of O_2 at low temperature leads to no spectroscopic changes, and even at room temperature, there is no immediate color change. Demetallation after 1 day following a **2**/O_2 reaction showed that the ligand remained unaffected (Scheme 2). Thus, a seemingly minor ligand

(82) Karlin, K. D.; Gultneh, Y.; Hayes, J. C.; Cruse, R. W.; McKown, J. W.; Hutchinson, J. P.; Zubieta, J. *J. Am. Chem. Soc.* **1984**, *106*, 2121−2128.
(83) Itoh, S.; Nakao, H.; Berreau, L. M.; Kondo, T.; Komatsu, M.; Fukuzumi, S. *J. Am. Chem. Soc.* **1998**, *120*, 2890−2899.
(84) Mahapatra, S.; Halfen, J. A.; Tolman, W. B. *J. Am. Chem. Soc.* **1996**, *118*, 11575−11586.
(85) Hatcher, L. Q.; Karlin, K. D. *J. Biol. Inorg. Chem.* **2004**, *9*, 669−683.
(86) Paul, P. P.; Tyeklár, Z.; Jacobson, R. R.; Karlin, K. D. *J. Am. Chem. Soc.* **1991**, *113*, 5322−5332.
(87) Wick, P. K.; Karlin, K. D.; Suzuki, M.; Zuberbuhler, A. D. *Micron* **2004**, *35*, 137−139.
(88) Wick, P. K.; Karlin, K. D.; et al. Manuscript in preparation.
(89) Taki, M.; Itoh, S.; Fukuzumi, S. *J. Am. Chem. Soc.* **2002**, *124*, 998−1002.

modification (i.e., the change/addition of one methylene group), essentially shuts off copper-mediated O_2 chemistry. We presume this has to do with the positively shifted redox potential of **2** (vide supra), precluding binding of O_2 to Cu(I); the latter process requires a significant degree of copper-to-O_2 electron-transfer.[2,90] As noted (see Introduction), the closely related ligand **C** was apparently not examined for Cu^I/O_2 reactivity but did undergo H_2O_2 mediated ligand−copper(II) complex sulfoxidation.[28]

Conclusion

We have performed the first systematic study of the effects of a thioether donor on the properties and chemistry of copper(I) complexes and on their O_2 reactivity, in direct comparison to closely related copper(I) complexes having a pyridyl ligand donor counterpart. We observe here that the sulfur donor raises the redox potential of **1-ClO$_4$** by ∼0.15 V versus the analogous $[Cu^I(TMPA)(MeCN)]^+$ copper(I) complex. Despite this increase in $E_{1/2}$, **1** reacts with O_2 at low temperature to generate the first copper−dioxygen adduct also possessing thioether ligation, an "end-on" peroxo complex, **4**, proven from EXAFS spectroscopy to possess $Cu-S_{thioether}$ bonding. This possesses a novel absorption spectrum depicting an additional π^*_v−Cu(II) transition indicating distortion away from trigonal bipyramidal structure. rR data for **4** show that Cu−O and O−O stretching frequencies are lowered in comparison to those of **5**. Thus, the thioether ligand weakens the Cu−O and O−O bonds by imposing a structural modification and/or by providing greater electron density to the Cu^{II} center relative to the nitrogen donors in TMPA. As discussed, enhanced thioether donation/structural distortion thus may contribute to Cu^{II}−superoxo active-species formation and stabilization at the DβH or PHM Cu_M site.

1/O_2 displays monooxygenase activity at room temperature whereby 44% (out of a 50% theoretical maximum) of the total ligand recovered after a $Cu^I + O_2$ reaction is the ligand-derived sulfoxide product. The same is observed for the reaction of **3** with H_2O_2 but in higher yields. As discussed above, DβH and PHM are unique copper-containing enzymes because of their chemistry occurring at a mononuclear copper site with an accompanying Met sulfur ligand. Thus, it may seem surprising that DβH or PHM Cu_M site destruction (via irreversible sulfoxide formation) does not appear to occur. This may be due to (i) the lack of facile electron transfer from the distant Cu_H (which could lead to a peroxide level intermediate) and (ii) very tight control and coupling of active species formation with substrate attack,[13] such that no leakage of reactive oxygen species occurs. Further structural, spectroscopic, and reactivity mechanistic studies are warranted in order to generate synthetically derived mononuclear copper−dioxygen adducts possessing thioether−nitrogen ligands, i.e., models for the leading candidates for active-site reactive intermediates.

The chemistry presented here also has some relevance to the methionine oxidation implicated in the oxidative stress pathogenesis of Alzheimer's disease (AD)[91,92] and other age-related diseases.[93] Amyloid β-peptides (Aβ, 1−42 residues in length) can coordinate copper and lead to the generation of reactive oxygen species (ROS) and cell toxicity.[94−96] The chemistry (sulfoxidation, or not) of Met-35 appears to be crucial in neurotoxic situations and in polymer/plaque formation; Met-sulfoxides are found in AD amyloid plaques.[97,98] In fact, methionine oxidation appears to be a recurrent theme in biology (formed quite likely from ROSs and redox metal mediated processes) and protein Met residues may be present as sacrificial reductants to scavenge ROSs and then be recycled back with methionine sulfoxide reductases.[93,99] Methionine oxidation is also implicated in cellular regulation.[100,101] Thus, the study of copper ion mediated sulfoxidation chemistry has a strong biological basis.

Future studies of copper−thioether complexes and their reactivity with O_2 and H_2O_2 may further contribute to our understanding of enzymatic and other biological processes.

Acknowledgment. We are grateful to the National Institutes of Health (K.D.K., GM28962; E.I.S., DK31450; K.O.H, RR-01209) for support of this research. SSRL operations are funded by the Department of Energy, Office of Basic Energy Sciences. The SSRL Structural Molecular Biology program is supported by the National Institutes of Health, National Center for Research Resources, Biomedical Technology Program, and by the Department of Energy, Office of Biological and Environmental Research.

Supporting Information Available: Crystallographic information file (CIF) of **1-(B(C$_6$F$_5$)$_4$)$_2$** and **3**, EPR spectrum of **3** and IR spectrum of **1-CO**. This material is available free of charge via the Internet at http://pubs.acs.org.

IC700541K

(90) Mirica, L. M.; Rudd, D. J.; Vance, M. A.; Solomon, E. I.; Hodgson, K. O.; Hedman, B.; Stack, T. D. P. *J. Am. Chem. Soc.* **2006**, *128*, 2654−2665.

(91) Butterfield, D. A.; Boyd-Kimball, D. *Biochim. Biophys. Acta* **2005**, *1703*, 149−156.

(92) Butterfield, D. A.; Bush, A. I. *Neurobiol. Aging* **2004**, *25*, 563−568.

(93) Stadtman, E. R. *Arch. Biochem. Biophys.* **2004**, *423*, 2−5.

(94) Ali, F. E. A.; Barnham, K. J.; Barrow, C. J.; Separovic, F. *Aust. J. Chem.* **2004**, *57*, 511−518.

(95) da Silva, G. F. Z.; Tay, W. M.; Ming, L. J. *J. Biol. Chem.* **2005**, *280*, 16601−16609.

(96) Huang, X.; Atwood, C. S.; Hartshorn, M. A.; Multhaup, G.; Goldstein, L. E.; Scarpa, R. C.; Cuajungco, M. P.; Gray, D. N.; Lim, J.; Moir, R. D.; Tanzi, R. E.; Bush, A. I. *Biochemistry* **1999**, *38*, 7609−7616.

(97) Schoneich, C. *Arch. Biochem. Biophys.* **2002**, *397*, 370−376.

(98) Varadarajan, S.; Kanski, J.; Aksenova, M.; Lauderback, C.; Butterfield, D. A. *J. Am. Chem. Soc.* **2001**, *123*, 5625−5631.

(99) Moskovitz, J. *Biochim. Biophys. Acta* **2005**, *1703*, 213−219.

(100) Bigelow, D. J.; Squier, T. C. *Biochim. Biophys. Acta* **2005**, *1703*, 121−134.

(101) Stadtman, E. R.; Van Remmen, H.; Richardson, A.; Wehr, N. B.; Levine, R. L. *Biochim. Biophys. Acta* **2005**, *1703*, 135−140.